The Hydrodynamic Cavitation Manifestation in Small Chips

Morteza Ghorbani (mortezag@kth.se)
Royal Institute of Technology

Research Article

Keywords: Cavitation, Small microchannel, Pressure, Surface roughness, Side wall roughness

Posted Date: May 6th, 2021

DOI: https://doi.org/10.21203/rs.3.rs-489442/v1

Version of Record: A version of this preprint was published at IEEE Access on August 6th, 2021. See the published version at https://doi.org/10.1109/ACCESS.2021.3102898.

The Hydrodynamic Cavitation Manifestation in Small Chips

Morteza Ghorbani [1,2,3,*]

[1]Department of Biomedical Engineering and Health Systems, KTH Royal Institute of Technology, SE-141 57 Stockholm, Sweden

[2]Sabanci University Nanotechnology Research and Application Center, 34956 Tuzla, Istanbul, Turkey

[3]Center of Excellence for Functional Surfaces and Interfaces for Nano-Diagnostics (EFSUN), Sabanci University, Orhanli, 34956, Tuzla, Istanbul, Turkey

*Correspondence: mortezag@kth.se

Abstract: Cavitation is a phase change phenomenon created by the static pressure reduction of a liquid medium at a constant temperature. This process has been considered as a disadvantageous mechanism in most turbomachinery systems, however, its potential in releasing energy at the bubble collapse stage has received lots of attention in recent decades. Particularly, the applicability of this phenomenon in micro scale gives rise to the research studies in different fields, i.e., wastewater treatment and medical imaging. In this study, microfluidic devices housing small microchannels have been fabricated to study the generation of the cavitating flow patterns bubbles. The main focuses in this work are on the surface and side wall roughness together with the size reduction effects on cavitation bubble generation. Accordingly, the microfluidic devices were fabricated using the techniques adopted from semiconductor based micro- fabrication. The experiments were performed at relatively higher upstream pressure, 4 to 7 MPa, to investigate the durability of the devices and flow patterns features. The results show that the side wall roughness elements are very effective in the small microchannels in terms of facile cavitating flow generation, while the size reduction in the diameter of the channel does not accompany intensified cavitating flow necessarily.

Keywords: Cavitation; Small microchannel; Pressure; Surface roughness; Side wall roughness

1. Introduction

Inertial cavitation includes the combination of chemical and physical effects, which appear in a cyclic form of generation, growth and collapse of bubbles. This type of cavitation which is observed in both hydrodynamic and acoustic is ended with an enormous energy release at the stage of the bubble implosion. Therefore, it is possible to utilize this energy in applications where substantial impact pressure of the bubbles is required for fragmentation or erosion of a surface, particle or material [1].

Hydrodynamic cavitation, in this regard, has been mostly considered as a negative mechanism due to its destructive effect on machinery systems [2]. However, the versatile nature of the cavitation bubbles especially in the diesel injection engines [3] in terms of better combustion performance, high quality atomization and less emission has opened many other windows to this phenomenon in a positive way, i.e., energy harvesting [4], biomedical application [5,6] and wastewater treatment [7].

Most of the above-mentioned applications have been benefitted from the concept of the "hydrodynamic cavitation on chip", which is originated from microfluidics [8]. This concept which has been emerged during the 2000s [9] and has been developed in the recent decade [10], exhibits an entirely different physics compared to its macro scale counterpart. Therefore, the preliminary studies in this regard, were mostly attributed to the cavitation physics and scrutinizing the bubble creation and the flow pattern classifications in micro scale [11,12].

Recently, some attempts to employ the microfluidic devices capable of generating hydrodynamic cavitation have been made in liquid phase exfoliation [13], chemiluminescence [14] and bacteria disinfection [15]. These studies have revealed the extensive and almost intact potential of hydrodynamic cavitation in microfluidics. Thus, it is timely to assess the micro scale cavitation strength in the emerging fields to design and fabricate new generation reactors influenced by the destructive payload of the micro bubbles.

The exploitation of hydrodynamic cavitation as a tool for biological wastewater treatment leads to the elimination of the thermal methods required in the wastewater treatment plants. It is due to the fact that, in addition to the free hydroxyl radicals and shockwaves, high temperature hot spots are the direct outcome of the bubble collapse as its thermal effect. This was shown in the disinfection rate of E. Coli in water with the aid of hydrodynamic cavitation when the temperature of the medium is changed [15].

Going back to the pioneering studies in the field, Mishra et al. [9], investigated the hydrodynamics cavitation in a micro-orifice which was located in a microchannel. They observed that as the cavitation number decreases, the various flow regimes are formed similar to the macro scale cavitation. In this study, the incipient cavitation number was very low which illustrated the effect of the size of the orifice. They also found a lower value for the choked cavitation numbers in microscale cavitating flows despite the pressure and velocity variations. They also recorded a fast transition in the flow patterns from inception choked and also from choked to supercavitation flow regime. Mishra et al. [16], continued their studies by observing the cavitating flow patterns in the flow of DI water as the working fluid through a short, sharp edged rectangular micro-orifice plate entrapped in a microchannel. They found that two thin vapor pockets/bubbles generated as an incipient cavitation phenomenon emerge from the center of the orifice plate boundaries. They showed that the twin

vapor pockets extended downstream by reducing the cavitation number and formed a curve interface between liquid and the vapor pockets. They illustrated the unique cavitating flow pattern which is significantly different from their macro scale counterparts.

The cavitating flow patterns from inception to fully developed cavitating flows are strongly affected by the surface roughness and the geometry of the orifice such as diameter, length and entrance shape. In this regard, Sarc et al. [17] investigated the cavitation bubble dynamics and intensity by considering the orifice geometry and configuration. Im et al. [18] also showed that the geometry of the orifice is very effective in the mean of intense cavitating flow pattern. In addition, the surface roughness elements have substantial effects of the generation of the facile cavitating flow pattern. Ghorbani et al. [19] investigated microscale hydrodynamic cavitation in a roughened device and found that devices with roughness elements could provide earlier cavitation inception.

The micro scale cavitating flow pattern has been studied in a wide range of Reynolds numbers from 100 to 100000 during recent years. Ghorbani et al. [8, 19, 20], in this regard, developed high pressurized microfluidic devices which could work at the upstream pressure higher than 6 MPa and extended the relevant studies which were performed at lower Reynolds numbers [9,21]. Their studies demonstrated that, there still needs in-depth investigations to reveal the surface roughness effects on the generation of the micro cavitation phenomenon reaching an optimum configuration for the desired microfluidic device.

In this study, microfluidic devices housing small microchannels were fabricated to investigate the surface and side wall roughness elements effects along with the size reduction effects on the generation of the cavitation bubbles. The first section of this study is devoted to the roughness effects in the small microchannels with the hydraulic diameter, D_H between 50 to 100 μm ($D_H = 4A/P$, where A is the cross-sectional area and P is the perimeter of the microchannel). The hydraulic diameter is slightly changed for some cases in which the surface roughness is applied. This section provides valuable insights into the side wall roughness impacts on the cavitation generation in small microchannels with non-dimensional numbers, i.e., cavitation number ($\sigma = (P_{ref} - P_v)/0.5\rho_l V_{ref}^2$, where ρ_l is liquid density, P_{ref} is reference pressure, which is the upstream pressure, P_{in} in this study, P_v is vapor saturation pressure and V_{ref} is the mean velocity of the flow inside the microchannel, which was calculated with the use of volume flow rate and cross sectional area) and Reynolds number ($Re = \rho v_{ref} D_H/\mu$, where μ is the liquid viscosity). In the second section, after demonstrating the strong effect of the side wall roughness effect, the cavitation phenomenon in four identical microfluidic devices with small microchannels, hydraulic diameters of 75 and 50 μm, were investigated. This study shows that reducing the microchannel hydraulic diameter does not provide a suitable condition for the cavitation generation necessarily, however, the small and short side wall roughness has a substantial effect in all the conditions.

2. Results

2.1. The surface and side wall roughness effects on the cavitation generation in small microchannels

In the first part of the study, cavitation is investigated inside the microchannel with various surface roughness elements at different upstream pressures, P_{in}. The surfaces of the microchannels have roughness elements height of 0 and 2 µm and, side wall roughness of 10 µm, while the hydraulic diameter of all devices is 100 µm. The results (Figures 1-3) show that the side wall roughness elements have substantial effects on the inception of the cavitation and development of the cavitating flow in small microfluidic devices compared to the surface roughness elements. Recently, it was demonstrated that apart from the working fluid inside microfluidic devices, surface roughness elements have a significant effect on the generation of cavitation bubbles [20]. Therefore, it is of great significance to investigate the surface characteristics by focusing on substrate nanoengineering techniques to achieve intense bubble generation and earlier cavitation inception to be utilized in energy and biomedical applications.

Figure 1 illustrates that for a plane surface, CH1, there is a very short length of cavitating flow inside the microchannel of the microfluidic device. The experiments were performed at various upstream pressures from 4 to 7 MPa, however, in spite of the high upstream pressure, a short cavitation footprint was recorded for this device. The experiments were carried out for an identical microfluidic device, CH2, with a surface roughness of 2 µm height to investigate the cavitation bubbles generation. The results of this device were presented in Figure 2, where cavitation inception was observed at upstream pressure of 4 MPa. Figure 2 shows that despite the pressure increase from 4 to 7 MPa, there is no substantial change in the flow regime appearance inside the microchannel. The cavitating flow does not develop along the microchannel. These results indicate that although the cavitation bubbles do not reach to the end of the channel and the supercavitation flow regime does not form, the case of CH1 with a smooth surface is capable of more intense generation of cavitation bubbles.

Further studies were performed with a microfluidic device housing a side wall roughness of 10 µm under the same conditions as in the previous devices. Figure 3 exhibits various cavitating flow regimes inside the CH3 at upstream pressures between 4 to 7 MPa. Accordingly, the cavitation bubbles extended to the outlet of the microchannel even at the upstream pressure of 5.5 MPa, while the supercavitation flow regime was observed at high upstream pressure of 7 MPa. Figure 3-a shows a clear separation of the twin cavities from the walls of the channel, while the side wall roughness is presented inside the microchannel.

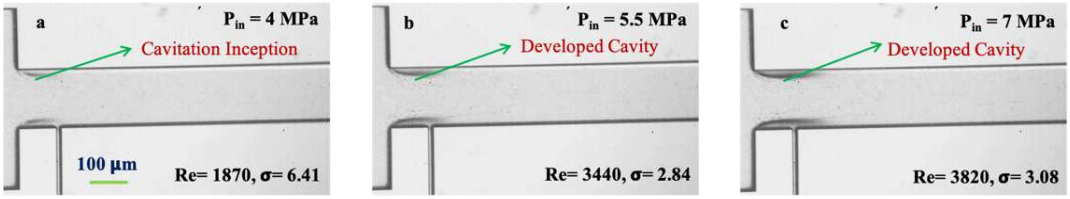

Figure 1. Fluid flow inside the microfluidic device (CH1) with smooth surface at different upstream pressures (P_{in})

The pattern for the side wall roughened channel corresponds to fully developed super-cavitation at an inlet pressure of 5.5 MPa, which is not seen in the other channels with surface roughness elements of 0 and 2 μm at this pressure (shown in Figure 1 and 2). Therefore, it could be concluded that similar to the bigger microfluidic devices [8], side wall roughness leads to early transitions between flow patterns even at smaller devices.

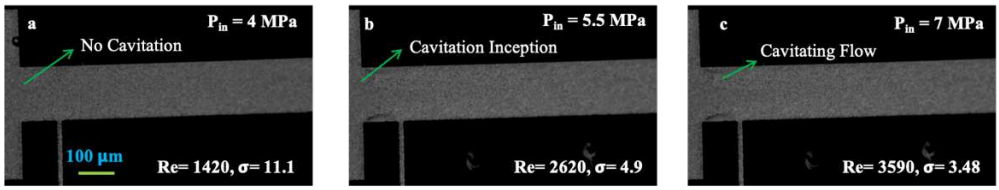

Figure 2. Cavitating flow inside the microfluidic device (CH2) with 2 μm surface roughness at different upstream pressures (P_{in})

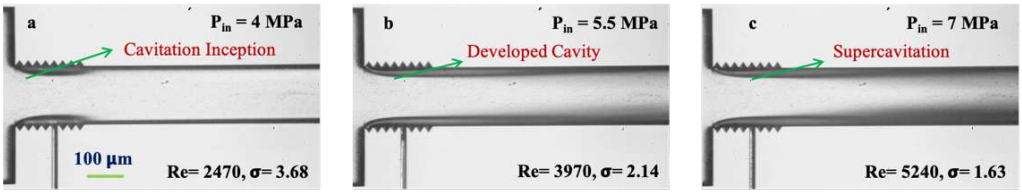

Figure 3. Cavitating flow inside the microfluidic device (CH3) with 10 μm side wall roughness at different upstream pressures (P_{in})

Figure 4 presents the cavitation number variations for CH1, CH2 and CH3 at different upstream pressures. The cavitation number which is an indication for the cavitation intensity provides valuable insight into the bubble that exists in the working area. The higher and lower values of this number indicate a lower and higher possibility of cavitation bubbles existence, respectively. Accordingly, the lower values of cavitation number for the case of CH3 demonstrate the higher amounts of the cavitation bubbles in this channel compared to the other devices. The decreasing of the cavitation number at different upstream pressures for the case of CH3 has a mild trend indicating that the mean velocity at the lower upstream pressure is even high compared to the other cases. This fact is also seen in Figure 5, where the Re numbers for lower upstream pressures is higher for the case of CH3. Therefore, the strong effects of the cavitation phenomenon on the velocity of the flow lead to higher Reynolds numbers at much lower upstream pressures. On the other hand, a sharp reduction in the cavitation number is observed for the other devices especially CH2 in which cavitation bubbles were barely visualized. This is due to the fact the velocity at higher upstream pressures increases substantially leads to a dramatic decrease in the cavitation number. Figure 5 illustrates the Reynolds number variations for the cases CH1, CH2 and CH3 with respect to the non-dimensional penetration length (x/L, x is the length of the cavitating flow inside the microchannel). The non-dimensional penetration length (x/L) which is calculated with the

aid of image processing software ImageJ is defined as the ratio of vapor cloud length to microchannel length. The results show that there is no considerable cavitating flow inside the device CH2, while the Re number at the highest upstream pressure is calculated as 3590. The Reynolds number in the identical situation for the case of CH3 is 5240 which exhibits the effects of the cavitation apparently. The Reynolds number for the case of CH1 is very close to CH2 (3820 as the highest value), however, the Reynolds numbers at the upstream pressure of 5.5 and 7 MPa are very close to each other implying that the cavitation intensity does not change considerably in the case of CH1 by increasing the upstream pressure. Therefore, side wall roughness elements height has the potential to create a suitable condition for the easier generation of cavitation bubbles and affects the turbulency of the flow at the lower upstream pressures even in the small microchannels.

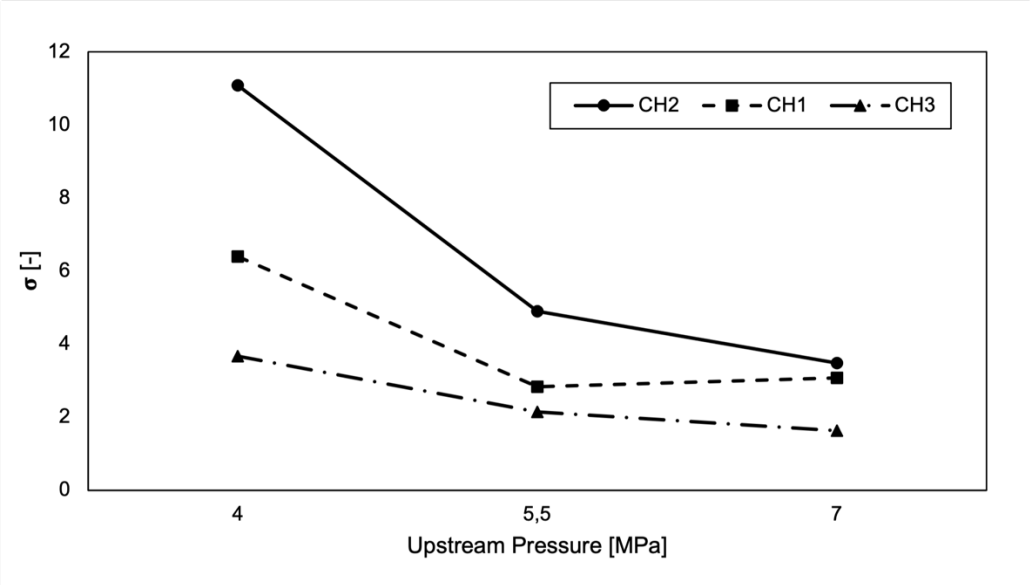

Figure 4. The variation of the cavitation number (**σ**) with respect to upstream pressure (P_{in}) for the microfluidic devices with different surface roughness elements height

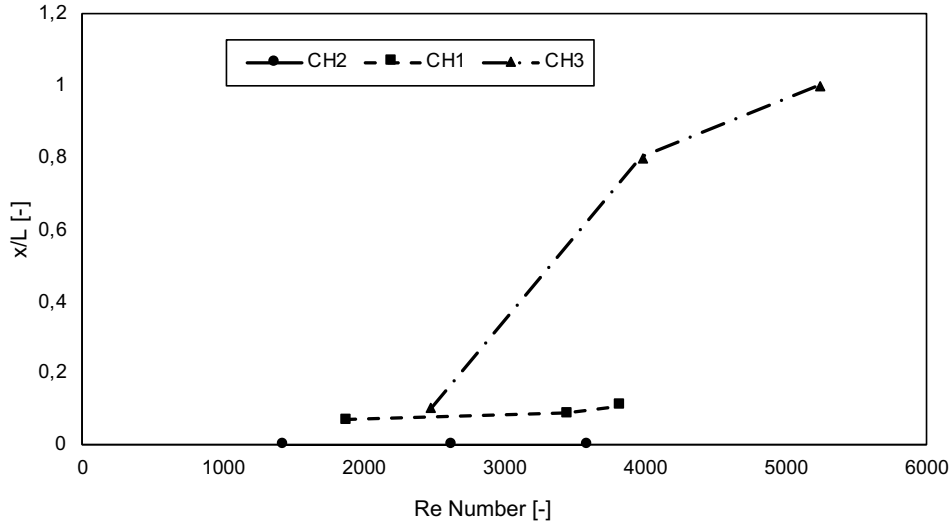

Figure 5. The variation of the non-dimensional penetration length with respect to Reynolds number for the micro-fluidic devices with different surface roughness elements height

2.2. The cavitation intensity in the small side wall roughened microchannels

The effect of the side wall roughness on the cavitating flow patterns was studied in the microfluidic devices in which the hydraulic diameters are far smaller than the devices fabricated in our previous studies [19,20]. The hydraulic diameters of these devices are 75 μm (CH4 and CH5) and 50 μm (CH6 and CH7) and the length of the roughness elements are the same while their heights are changing. The results show that the smaller and shorter side wall roughness elements have substantial effects on the generation of the facile cavitating flow patterns. In comparison to the microfluidic devices with larger microchannels (D_H=100 to 240 μm) in our previous studies [19,20], the cavitation inception is observed at higher pressure (3 MPa) and the corresponding cavitation number is also higher (2.01). Therefore, with a constant inlet channel width, reducing the hydraulic diameter of the microchannel leads to higher energy demand for the cavitation inception in micro scale. Further reduction in the hydraulic diameter of the microchannel results in less intense cavitation patterns even at higher pressures (Figure 6-g) and no cavitation in some cases (Figure 6-d and h). These results indicate that reducing the hydraulic diameter of the microchannel while the inlet channel is constant is not accompanying by a facile cavitating flow pattern and lower cavitation number. The detailed features of the cavitating flow patterns for the small microfluidic devices with side wall roughness elements (CH4, 5, 6 and 7) are presented in Figure 6. The results show that supercavitation occurs at higher upstream pressure in CH5 compared to CH4, however, the interesting point between these cases is that the cavitation numbers corresponding to Figures 6-e and f are 0.89 and 1.67, respectively. This fact means that at smaller microchannels, the intensity of the cavitating flow for the cases with bigger roughness elements is higher, which is in contrast to the larger microfluidic devices. On the other hand, the cavitation is not seen for the case of CH7 even at very high upstream pressures, let alone the cavitation in a similar channel with smaller roughness elements is not as facile as the cases of CH4 and CH5.

The cavitation feature is also shown in the extended channel of the microfluidic devices just after the microchannel for all the cases in Figure 7. Surprisingly, the twin cavities are observed in all the cases even for the case of CH7. The intensity of the cavitating flows inside the microchannel substantially affects the flow behavior in the extended channel of the device for the case of CH4, where the strong vortices lead to reattachment point movement in Figures 7-a and e. The downstream effects together with the rotating vortices and circulating bubbles create a significant hysteresis for this case. The twin cavities created in Figures 7-c and g are more facile compared to the other cases despite the relatively moderate features of the cavitation inside its microchannel. This indicates that the cavitating flow patterns inside the extended channel of the device could be independent of the upstream events and the downstream phenomena such as vortices and low-pressure regions affect the intensity of the cavitation. This is also interpreted from the cases of CH5 and CH7 in which cavitation has almost the same feature, while no cavitation is recorded in the case of CH7.

Figure 8 illustrates the variation of the P_2, the pressure at the location of the vena contracta, with respect to the pressure drop between the upstream pressure and P_2. The pressure at the location of the vena contracta is an indication of the bubble generation inception, however, this location may change according to the device geometry and thermophysical condition of the flow. The vena contracta in some reports is defined as the $1D_H$

[22], and this value is considered as a reference point in the current study. The results exhibit low pressure drop requirement for the cavitation inception for the case of CH4 in which the pressure at the location of the vena contracta is also low compared to the other cases. After the cavitation inception for the case of CH4, the P_2 is reduced to lower values compared to the vapor saturation pressure of water (2300 Pa) with increasing the pressure drop. This fact indicates the intense cavitating flow condition. The cavitation inception is observed at higher pressures at the location of the vena contracta (around 1.5 MPa) for the cases of CH5 and CH6, while there needs much more pressure drop (around 4 MPa). The P_2 reduces to the values lower than the vapor saturation pressure after the cavitation inception for these cases, however, there need high energy inputs to reach the intense cavitation condition for the cases of CH5 and CH6. The results corresponding to the pressure drop and P_2 presented for the case of CH7 are shown that the P_2 is increased by the pressure drop rise implying that the cavitation phenomenon does not happen in this case.

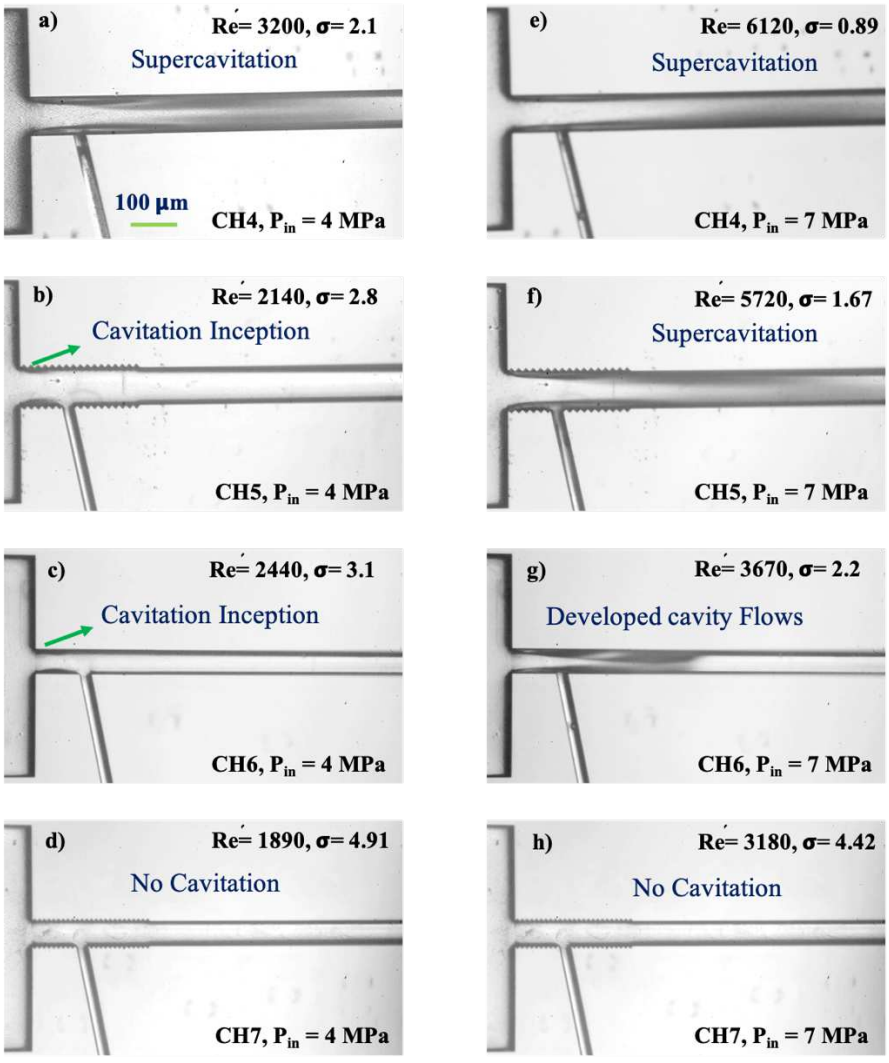

Figure 6. The occurrence of the cavitating flow patterns inside four different microfluidic devices at upstream pressures (P_{in}) of 4 and 7 MPa

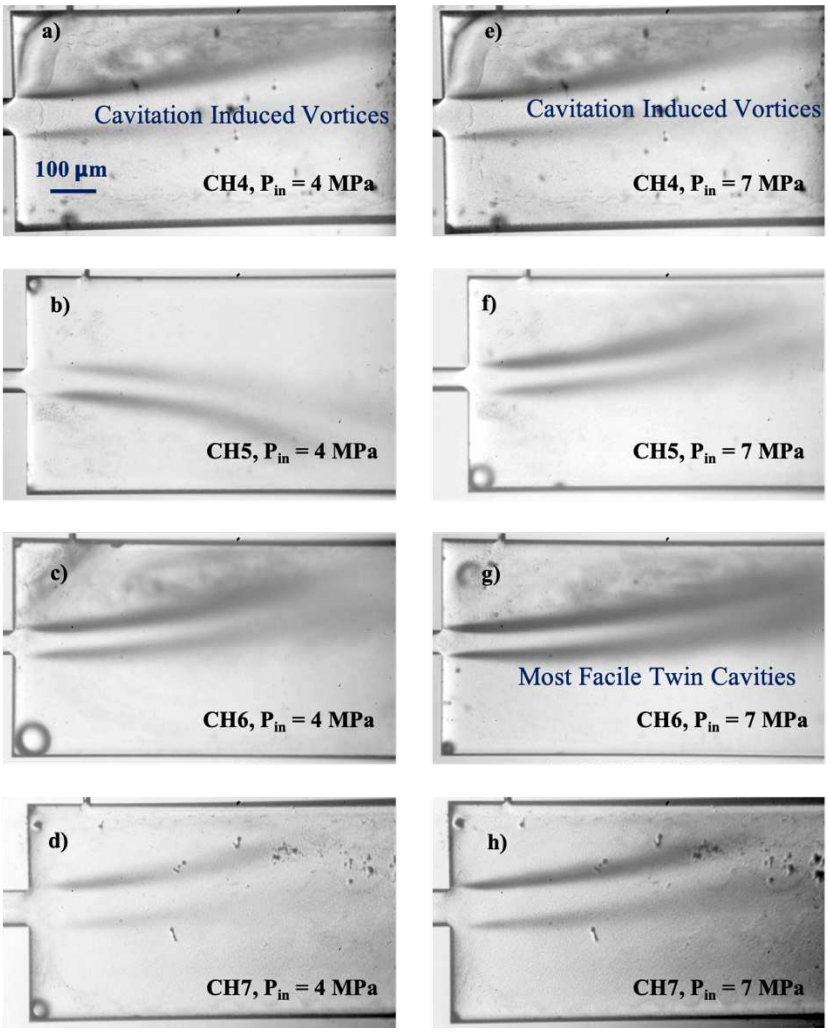

Figure 7. The twin cavities in the extension part of the four side wall roughened microfluidic devices at upstream pressures (P_{in}) of 4 and 7 MPa

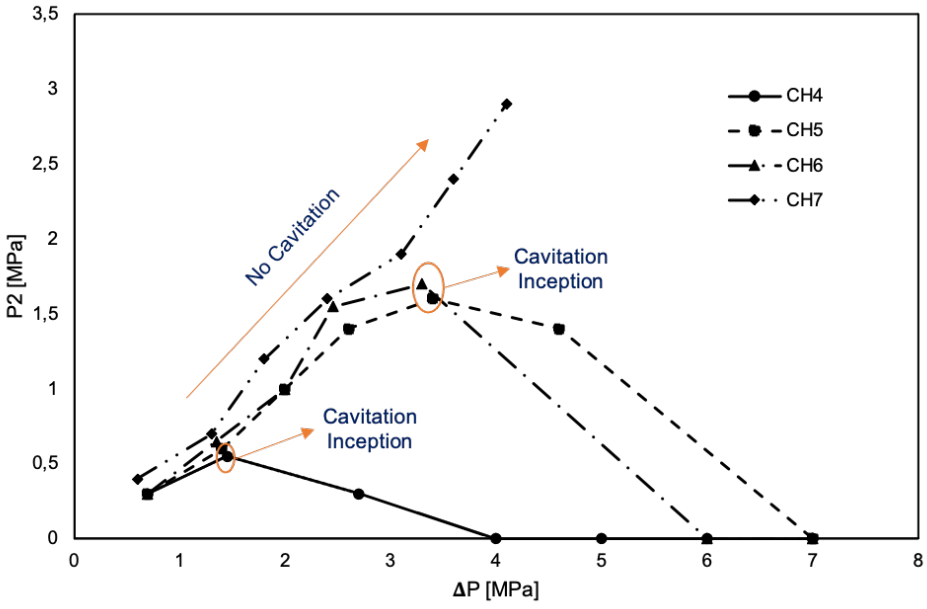

Figure 8. The variation of the P2, the pressure at the location of the vena contracta with respect to the pressure drop for four side wall roughened microfluidic devices

3. Discussion

Cavitation usually happens due to rapid pressure reduction. In the case of the extended channel, by flow injection from microchannel inside the bigger space, the localized low pressures together with high shear forces induces the cavitating flow. The cavitating flow entered the extended channels is accompanied with generation of low-pressure regions particularly on the below and above the twin cavities. The pressure reduction together with the surface tension effects in this region leads to the creations of the vortices which are mostly departed from the surface. The small bubbles grow in the cyclic form in this region and encounter with region with high pressure and finally collapse. This rapid change of nozzle size has a direct influence on both pressure and velocity which may cause cavitation and they are most probable and visible in the area in which changes are higher such as the boundary of the jet inside the channel. The movement and direction of flow depend on several parameters. Other terms can be the effect of the downstream nozzle. There are also some other phenomena such as step flow and wake area in the corner of the channel can create a periodic movement of the jet with low frequency due to separation effect (similar to Karman vortex phenomenon) and it could eventually become stronger and lean jet to direction creation.

In this study, the cavitation phenomenon inside microfluidic devices with different roughness elements was studied. It is shown that the cavitation bubbles are easily generated inside small microchannels with short and small side wall roughness elements. Accordingly, it is possible to reach developed cavitating flows and supercavitation conditions in a side wall roughened microfluidic device at a significantly lower upstream pressure. In addition, it is illustrated that the surface roughness does not have a significant effect on the generation of cavitation bubbles. In contrary to the surface roughened devices, the plane small microfluidic devices are capable of generating cavitation bubbles at higher pressures, which is still less efficient in comparison with the side wall roughened devices. Further investigations on the small microfluidic devices having short side wall roughness elements reveal that small roughness elements have a considerable effect on the cavitation bubble generation, while the hydraulic diameter reduction does not provide the same effects.

4. Materials and Methods

Seven microfluidic devices with very small hydraulic diameter have been designed and fabricated to study the occurrence of the cavitation phenomenon in microscale. The fabrication process is very sensitive to the design, geometry, and roughness. Therefore, extensive information about the process and flow condition is required. Accordingly, the geometrical specifications of the microfluidic devices capable of generating cavitation phenomenon should be investigated in broad ranges to generate cavitation, turbulence, and fluid flow patterns inside the microchannels with respect to the fabrication process.

The uncertainties found in the experimental devices and parameters were presented by the manufacturer's specification sheets or were obtained using the propagation of uncertainty method presented in the work of Kline and McClintock [23]. Accordingly, the average uncertainties in cavitation number (±6.8%), flow rate (±1.4%), inner diameter (±0.2 μm) and pressure drop (±0.3%) were calculated.

4.1 Design and Fabrication of Microfluidic Device

The thicknesses of the silicon and glass wafers are 760 μm which makes the microfluidic device thick enough to withstand high shear rates produced by bubble collapse as a result of the pressure drop. In addition, in this design, silicon wafers experienced the wet etching process for the formation for the orifice configurations. The typical microchannels do not mostly have the enough rigidity to tolerate the high pressures or do not have an access for optical measurement, which is vital for microscale cavitation studies. Certain non-intrusive techniques were utilized to optically characterize flows and cavitation inside microchannels at elevated pressures.

Fabrication and development of the device configurations having small flow restrictive element with micro size inner hydraulic diameters of 100, 75 and 50 μm (lengths of 2 mm) are based on our previous studies with hydraulic diameters in the range of 133 to 300 μm [20,24]. The devices which are made of silicon and glass wafers are highly durable to high pressure drops between inlet and outlet. This helps us to increase the upstream pressure (typically the researchers choose different ways around for the cavitation number calculation. One way to generate the cavitation is to decrease the downstream pressure while the upstream pressure is constant. In this case, it is the downstream pressure which is considered as the reference pressure. The other way which was also used in this study is to increase the upstream pressure while the downstream pressure is constant at atmospheric pressure. In the current study, the upstream pressure (which is the gauge pressure exactly at the beginning of the microchannel) was used as the reference pressure [19,20]) to reach high velocities which is important to study the turbulence effects. Accordingly, the microfluidic devices are produced on a double side polished <100> silicon wafer and have a bonding to a glass wafer. The main sections on the silicon part of the device are three channels- inlet channel, microchannel and extension as the outlet channel- and six holes including one inlet, two outlets and three pressure ports. First, PECVD (Plasma-enhanced chemical vapor deposition) is utilized to deposit a 50 nm thick layer of silicon dioxide on both sides of the silicon wafer, and photolithography and dry etching are performed in the next steps. The desired mask is patterned on the silicon layer to transfer the mask on the substrate and dry etching is carried outby adding the silicon dioxide layer. In the next step, the inlet, outlets, and pressure ports are transferred to the substrate for 200 μm with the use of dry etching, new layer is replaced by eliminating the photoresist layer. The second pattern is transferred on the silicon so that the microchannel has a connection to the etchant solutions. In the next, the new masked silicon is etched for 50 μm, and the final pattern is formed on the device. To avoid any dust and contaminant, the silicon underwent a wet etching process to prepare the substrate ready for the bonding step. The final step is to bond the substrate to the glass wafer to withstand high pressures. The anodic bonding is used for the bonding step to make the wafer durable enough for the high injection pressures. Figure 9 shows the entire flow process for the fabrication of the device. The microfluidic device specifications were presented in Table 1.

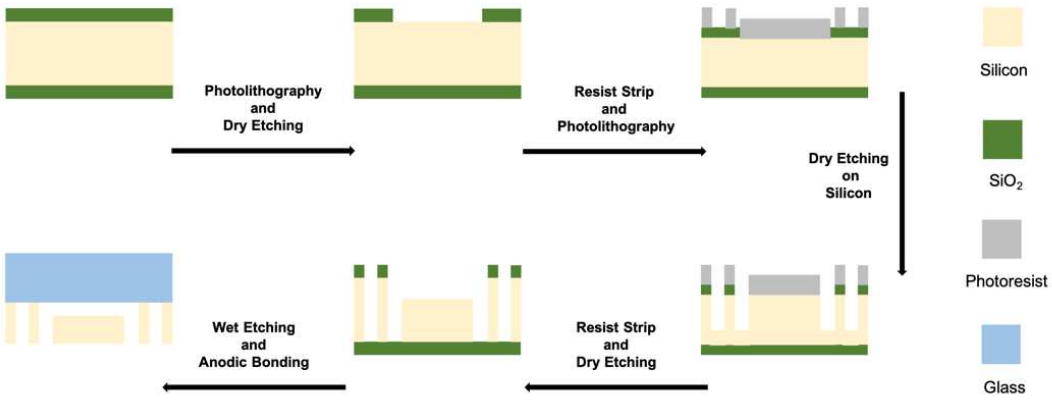

Figure 9. The process flow presenting the manufacturing process of the microfluidic devices

Table 1. The specifications of the microfluidic devices

Device	Hydraulic Diameter, D_H [μm]	Microchannel Length [mm]	Surface Roughness [μm]	Side Wall Roughness Height [μm]	Side Wall Roughness Length [mm]
CH1	100	2	0	0	0
CH2	100	2	2	0	0
CH3	100	2	0	10	0.66
CH4	75	2	0	0.75	0.66
CH5	75	2	0	7.5	0.66
CH6	50	2	0	0.5	0.66
CH7	50	2	0	5	0.66

4.2 Experimental Setup and Procedure

The microfluidic device is connected to the tubing system and fittings as shown in Figure 10. The input pressure is introduced to the container and tubing via a high-pressure pure nitrogen tank (Linde Gas, Gebze, Kocaeli). The nitrogen tank is connected to a 1 Gallon fluid container (Swagelok, Erbusco BS, Italy), filled with de-ionized (DI) water. The fluid reservoir is mounted to the system with appropriate fittings. Three pressure gauges (Omega, USA) are installed at the end of the experimental setup and on the sandwich to measure the pressures. One fine control valve (Swagelok) is mounted to the setup to control the flow along the system. To avoid any particles larger than 15 μm, a micro T-type filter (Swagelok) with a nominal pore size of 15 μm is mounted to the setup. A power LED source serves for illumination to have high quality records.

The inlet pressure varies between 4-7 MPa, while the temperature is constant at room temperature (approximately 21 ^{0}C). Although microchips have different roughness, they have the same inlet structure which

fits the same package. Micro-chips are sandwiched to the package with screw mechanisms to allow for withstanding inlet pressures of the liquid up to around 6 MPa. Liquid flow is controlled by valves at different locations. There are three pressure gauges on the setup to check for the pressure values, which are inlet, outlet, and channel pressures. Images are recorded with a CMOS camera, which has 1280x800 resolution with a short delay. The flow rate is measured and the effect of the discharge on the creation of the cavitation bubbles is obtained. The flow rate is measured by recording the level of the accumulated water level with respect to time.

The glass wafer helps in observing the flow inside the microchannels. The volumetric flow rate is raised with the alteration in the upstream pressure. The cavitating flow patterns inside the microchannel is captured at different zones in the microfluidic device. Different mechanical phenomena such as inception, developed cavities and supercavitation at the outlet of the microchannel are recorded by the high-speed visualization camera. The snaps of the cavitating flows are gathered by a double-shutter high-speed complementary metal-oxide semiconductor (CMOS) camera, which allows two successive frames to be visualized with a resolution of 1280 x 800 pixels (0.02 mm pixel size) within a short time delay [25-27]. A macro camera lens is mounted on the CMOS camera (type K2 DistaMax with focal length: s = 50 mm and f-number: f = 1.2) at a distance of 342 mm from the imaging plane, yielding a magnification of M = 0.137. These optical sequences make it possible that only the central zone of the lens is employed, where aberration can be neglected. The lightening is given to the system in front of the device to make the considered zone clear for the high-speed visualization system. The observation is performed in three main zones. The first zone is the microchannel, where the static pressure is expected to decrease to saturation vapor pressure. The second zone is the extended channel, where the twin cavities are emerged in. The last zone is the outlet channel, where the cavitating flows is encountered with.

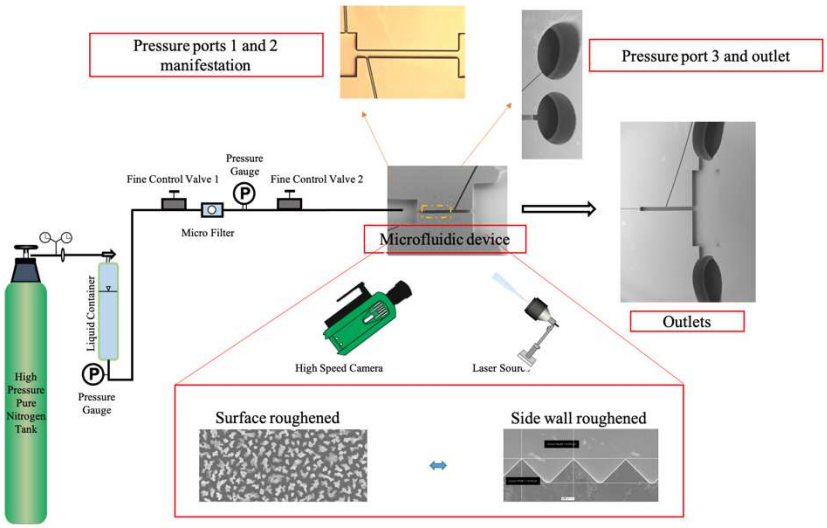

Figure 10. The experimental setup schematic illustrating the component required for the creation of the hydrodynamic cavitation phenomenon in a microfluidic device; The measured pressure in port 1 is P_{in} which is upstream pressure (also used as the reference pressure in the cavitation number formula), the P2 is measured at port 2, and the pressure measured at port 3 is approximately atmospheric pressure in all the cases.

References

1. Fu Y; Lu H; Nian G; Wang P; Lin N; Hu X; Zhou H; Yu H; Qu S; Yang W. Size-dependent inertial cavitation of soft materials. *Journal of the Mechanics and Physics of Solids* **2020**, *137*, 103859.
2. Gevari MT; Abbasiasl T; Niazi S; Ghorbani M; Koşar A. Direct and indirect thermal applications of hydrodynamic and acoustic cavitation: A review. *Applied Thermal Engineering* **2020,** *171*, 115065.
3. Shervani-Tabar MT; Parsa S; Ghorbani M. Numerical study on the effect of the cavitation phenomenon on the characteristics of fuel spray. *Mathematical and Computer Modelling* **2012**, *56(5-6),* 105-17.
4. Ghorbani M; Mohammadi A; Motezakker AR; Villanueva LG; Leblebici Y; Koşar A. Energy harvesting in microscale with cavitating flows. *ACS omega* **2017**, *2(10)*, 6870-7.
5. Ghorbani M; Oral O; Ekici S; Gozuacik D; Koşar A. Review on lithotripsy and cavitation in urinary stone therapy. *IEEE reviews in biomedical engineering* **2016,** *9*, 264-83.
6. Ghorbani M; Sozer C; Alcan G; Unel M; Ekici S;Uvet H; Koşar A. Biomedical device prototype based on small scale hydrodynamic cavitation. *AIP Advances* **2018,** *8(3)*, 035108.
7. Dular M; Griessler-Bulc T; Gutierrez-Aguirre I; Heath E; Kosjek T; Klemenčič AK; Oder M; Petkovšek M; Rački N; Ravnikar M; Šarc A. Use of hydrodynamic cavitation in (waste) water treatment. *Ultrasonics Sonochemistry* **2016**, *29*, 577-88.
8. Ghorbani M; Sadaghiani AK; Villanueva LG; Koşar A. Hydrodynamic cavitation in microfluidic devices with roughened surfaces. *Journal of Micromechanics and Microengineering* **2018**, *28(7)*, 075016.
9. Mishra C; Peles Y. Cavitation in flow through a micro-orifice inside a silicon microchannel. *Physics of fluids* **2005**, *17(1)*, 013601.
10. Medrano M; Zermatten PJ; Pellone C; Franc JP; Ayela F. Hydrodynamic cavitation in microsystems. I. Experiments with deionized water and nanofluids. *Physics of Fluids* **2011**, *23(12)*, 127103.
11. Ghorbani M; Sadaghiani AK; Yidiz M; Koşar A. Experimental and numerical investigations on spray structure under the effect of cavitation phenomenon in a microchannel. *Journal of Mechanical Science and Technology* **2017**, *31(1),* 235-47
12. Ghorbani M; Yildiz M; Gozuacik D; Kosar A. Cavitating nozzle flows in micro-and minichannels under the effect of turbulence. *Journal of Mechanical Science and Technology* **2016**, *30(6)*, 2565-81.
13. Qiu X; Bouchiat V; Colombet D; Ayela F. Liquid-phase exfoliation of graphite into graphene nanosheets in a hydrocavitating 'lab-on-a-chip'. RSC advances **2019**, *9(6)*, 3232-8.
14. Perrin L; Colombet D; Ayela F. Comparative study of luminescence and chemiluminescence in hydrodynamic cavitating flows and quantitative determination of hydroxyl radicals production. *Ultrasonics Sonochemistry* **2021**, *70*, 105277.
15. Gevari MT; Parlar A; Torabfam M; Koşar A; Yüce M; Ghorbani M. Influence of fluid properties on intensity of hydrodynamic cavitation and deactivation of Salmonella typhimurium. *Processes* **2020**, *8(3)*, 326.
16. Mishra C; Peles Y. An experimental investigation of hydrodynamic cavitation in micro-Venturis. *Physics of Fluids* **2006**, *18(10)*, 103603.

17. Šarc A; Stepišnik-Perdih T; Petkovšek M; Dular M. The issue of cavitation number value in studies of water treatment by hydrodynamic cavitation. *Ultrasonics sonochemistry* **2017**, *34*, 51-9.
18. Im KS; Cheong SK; Powell CF; Ming-chia DL; Wang J. Unraveling the geometry dependence of in-nozzle cavitation in high-pressure injectors. *Scientific reports*, **2013**, *3(1)*, 1-5.
19. Ghorbani M; Chen H; Villanueva LG; Grishenkov D; Koşar A. Intensifying cavitating flows in microfluidic devices with poly (vinyl alcohol)(PVA) microbubbles. *Physics of Fluids* **2018**, *30(10)*, 102001.
20. Ghorbani M; Deprem G; Ozdemir E; Motezakker AR; Villanueva LG; Koşar A. On "cavitation on chip" in microfluidic devices with surface and sidewall roughness elements. *Journal of microelectromechanical systems* **2019,** *28(5)*, 890-9.
21. Stieger T; Agha H; Schoen M; Mazza MG; Sengupta A. Hydrodynamic cavitation in Stokes flow of anisotropic fluids. *Nature communications* **2017**, *8(1)*, 1-1.
22. Emerson Automation Solutions, "Fundamentals of orifice meter measurement," White Paper, February 2017.
23. Kline SJ; McClintock FA. Describing uncertainties in single-sample experiments. *Mech. Eng* **1953**, *75*, 3–8.
24. Ghorbani M; Aghdam AS; Gevari MT; Koşar A; Cebeci FÇ; Grishenkov D; Svagan AJ. Facile hydrodynamic cavitation ON CHIP via cellulose nanofibers stabilized perfluorodroplets inside layer-by-layer assembled SLIPS surfaces. *Chemical Engineering Journal* **2020**, *382*, 122809.
25. Ghorbani M; Alcan G; Yilmaz D; Unel M; Kosar A. Visualization and image processing of spray structure under the effect of cavitation phenomenon. *Journal of Physics: Conference Series* **2015**, *656*, 012115.
26. Karimzadehkhouei M; Ghorbani M; Sezen M; Şendur K; Pınar Mengüç M; Leblebici Y; Koşar A. Increasing the stability of nanofluids with cavitating flows in micro orifices. *Applied Physics Letters* **2016**, *109(10)*, 104101.
27. Ghorbani M; Alcan G; Unel M; Gozuacik D; Ekici S; Uvet H; Sabanovic A; Kosar A. Visualization of microscale cavitating flow regimes via particle shadow sizing imaging and vision based estimation of the cone angle. *Experimental Thermal and Fluid Science* **2016**, *78*, 322-33.

Acknowledgements

This work was supported by TUBITAK (The Scientific and Technological Research Council of Turkey) Support Program for Scientific and Technological Research Project Grant No. 217M869. Equipment utilization support from Sabanci University Nanotechnology Research and Application Center (SUNUM) is gratefully appreciated.

Author Contributions

Conceptualization: MGH; Data curation: MGH; Formal analysis: MGH; Funding acquisition: MGH; Investigation: MGH; Methodology: MGH; Project administration: MGH; Resources: MGH; Software: MGH; Supervision: MGH; Validation: MGH; Visualization: MGH; Roles/Writing - original draft: MGH; Writing - review & editing: MGH.

Informed Consent Statement:

Not applicable.

Competing Interests Statement

The authors declare no conflict of interest.

Figure legends

Figure 1. Fluid flow inside the microfluidic device (CH1) with smooth surface at different upstream pressures

Figure 2. Cavitating flow inside the microfluidic device (CH2) with 2 μm surface roughness at different upstream pressures

Figure 3. Cavitating flow inside the microfluidic device (CH3) with 10 μm side wall roughness at different upstream pressures

Figure 4. The variation of the cavitation number (**σ**) with respect to upstream pressure for the microfluidic devices with different surface roughness elements height

Figure 5. The variation of the non-dimensional penetration length with respect to Reynolds number for the microfluidic devices with different surface roughness elements height

Figure 6. The occurrence of the cavitating flow patterns inside four different microfluidic devices at upstream pressures of 4 and 7 MPa

Figure 7. The twin cavities in the extension part of the four side wall roughened microfluidic devices at upstream pressures of 4 and 7 MPa

Figure 8. The variation of the P2, the pressure at the location of the vena contracta with respect to the pressure drop for four side wall roughened microfluidic devices

Figure 9. The process flow presenting the manufacturing process of the microfluidic devices

Figure 10. The experimental setup schematic illustrating the component required for the creation of the hydrodynamic cavitation phenomenon in a microfluidic device

Tables

Table 1. The specifications of the microfluidic devices

Device	Hydraulic Diameter, D_H [μm]	Microchannel Length [mm]	Surface Roughness [μm]	Side Wall Roughness Height [μm]	Side Wall Roughness Length [mm]
CH1	100	2	0	0	0
CH2	100	2	2	0	0
CH3	100	2	0	10	0.66
CH4	75	2	0	0.75	0.66
CH5	75	2	0	7.5	0.66
CH6	50	2	0	0.5	0.66
CH7	50	2	0	5	0.66

Figures

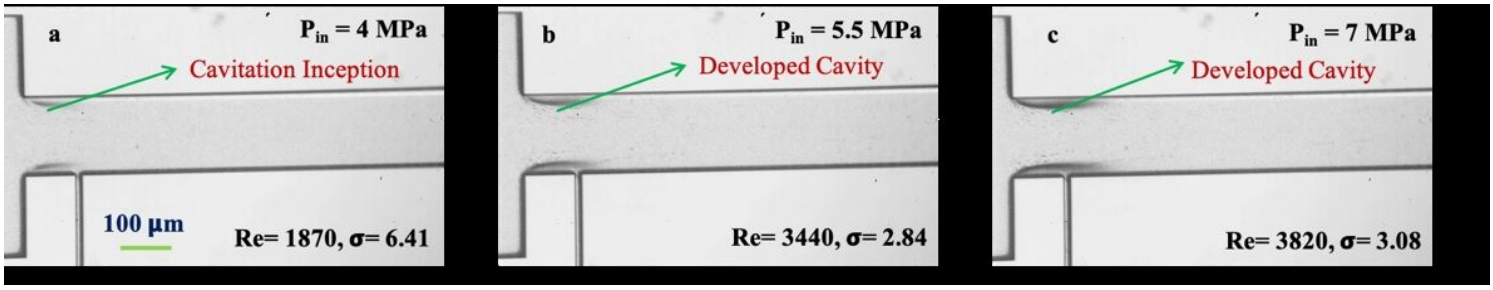

Figure 1

Fluid flow inside the microfluidic device (CH1) with smooth surface at different upstream pressures (Pin)

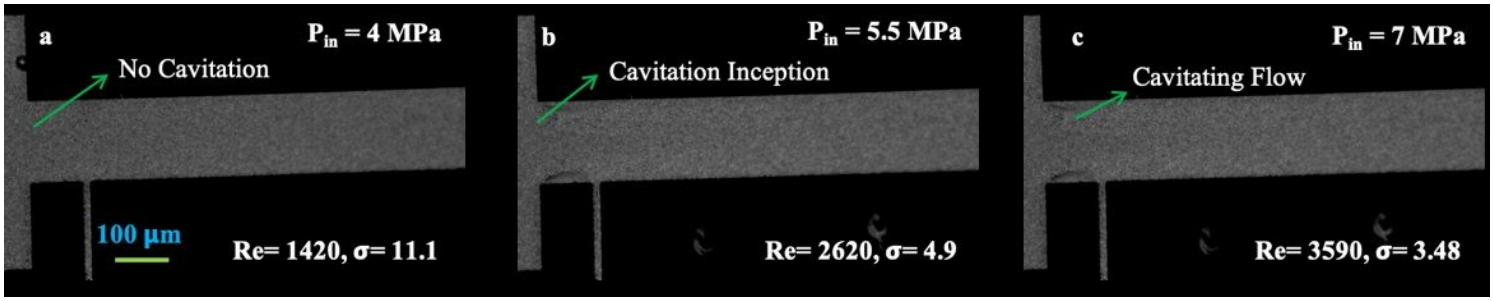

Figure 2

Cavitating flow inside the microfluidic device (CH2) with 2 µm surface roughness at different upstream pressures (Pin)

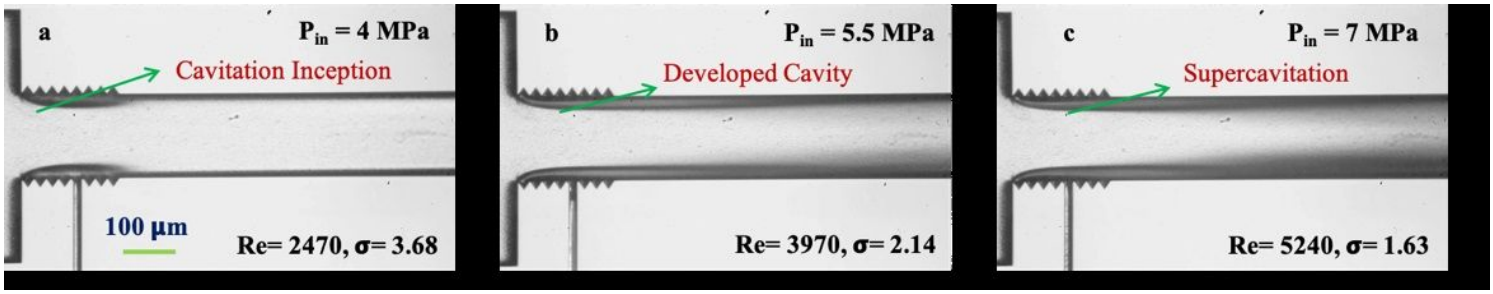

Figure 3

Cavitating flow inside the microfluidic device (CH3) with 10 µm side wall roughness at different upstream pressures (Pin)

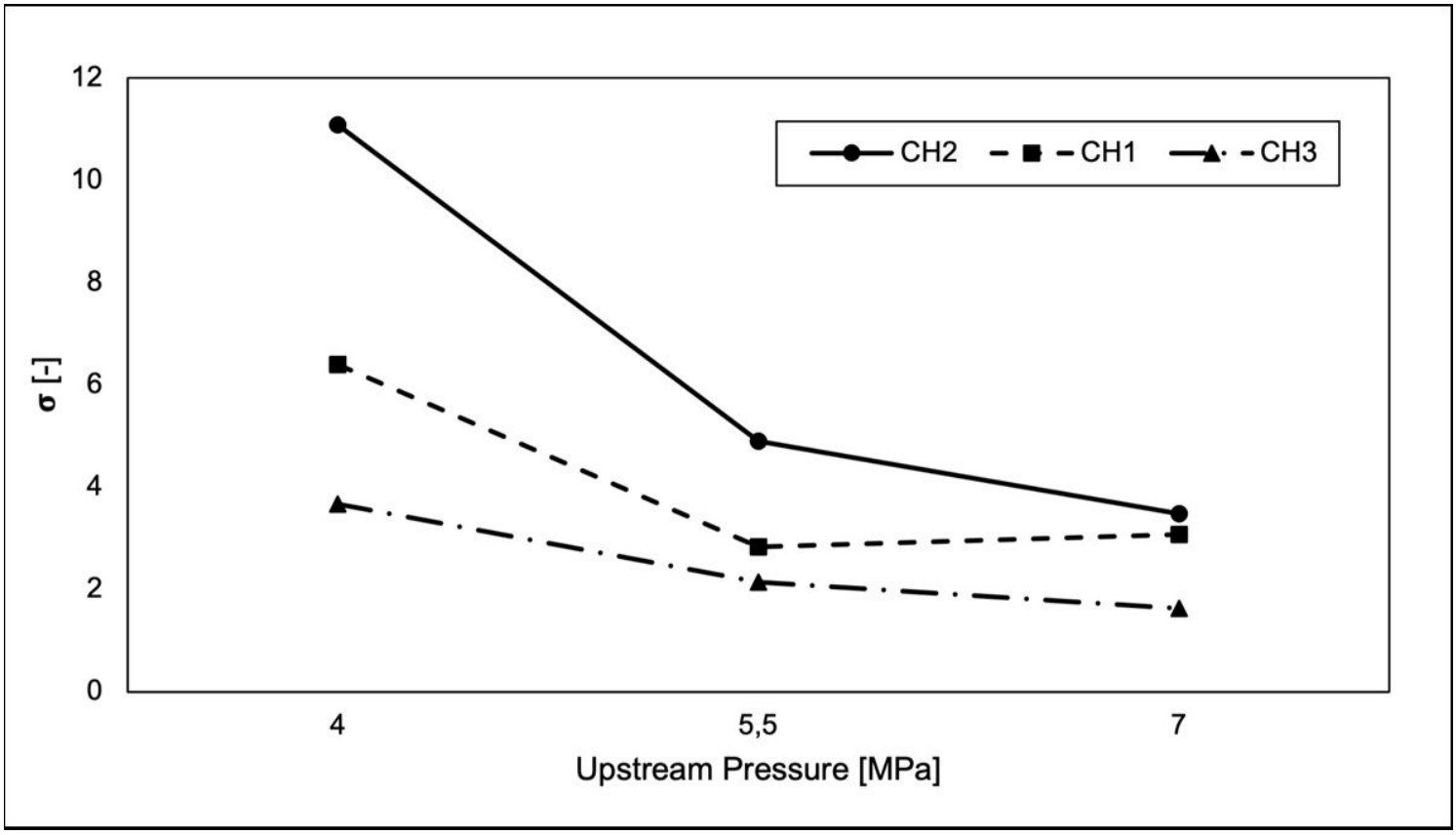

Figure 4

The variation of the cavitation number (□) with respect to upstream pressure (Pin) for the microfluidic devices with different surface roughness elements height

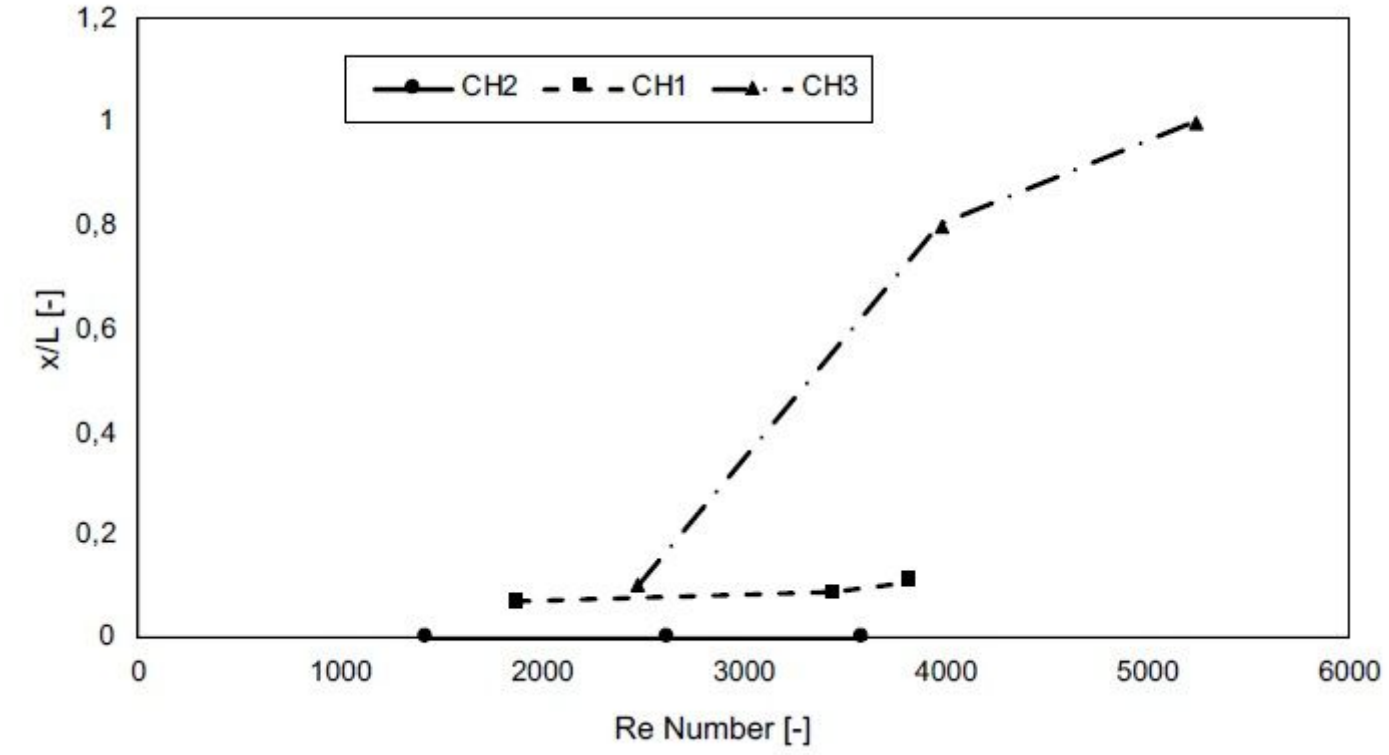

Figure 5

The variation of the non-dimensional penetration length with respect to Reynolds number for the microfluidic devices with different surface roughness elements height

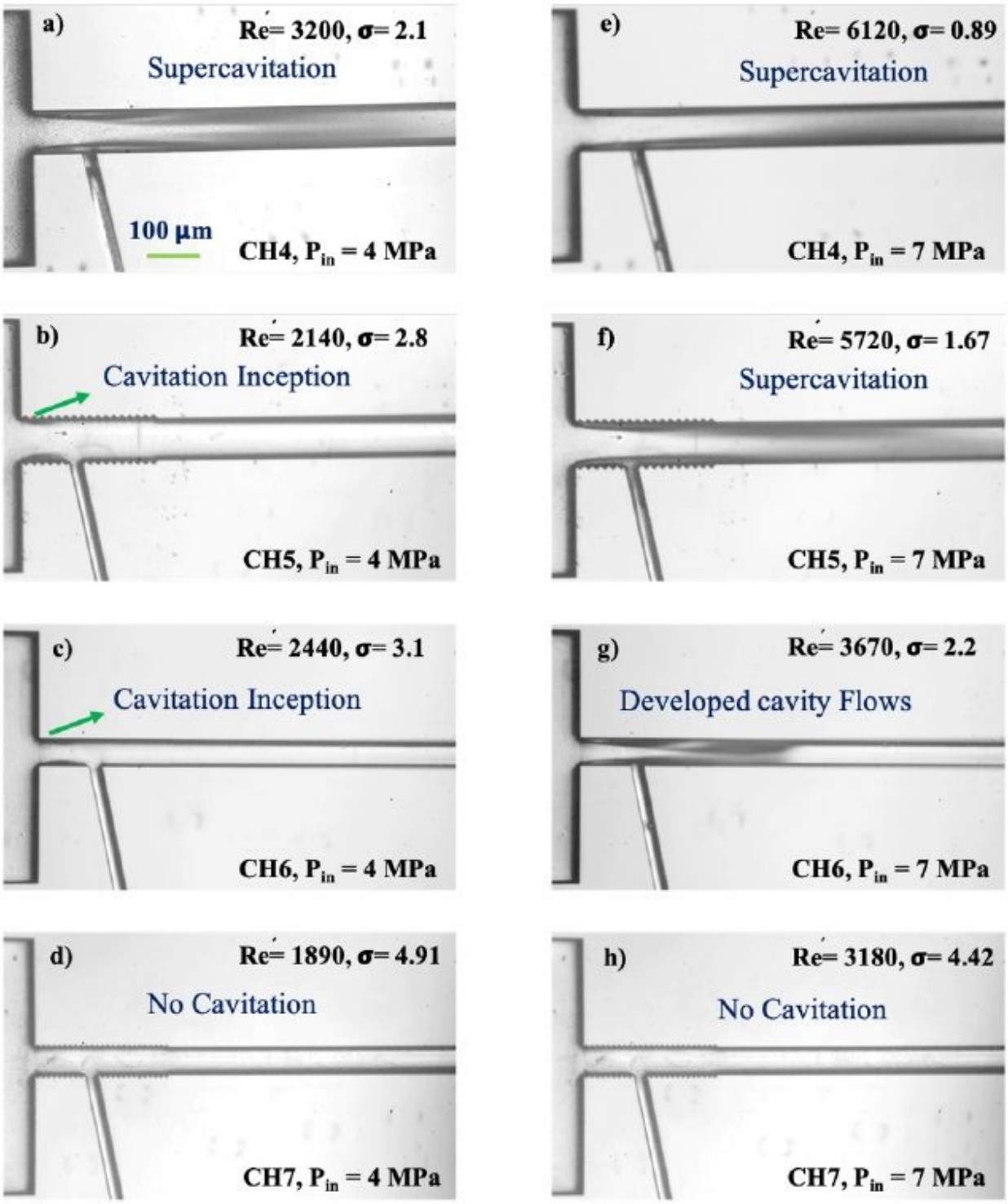

Figure 6

The occurrence of the cavitating flow patterns inside four different microfluidic devices at upstream pressures (Pin) of 4 and 7 MPa

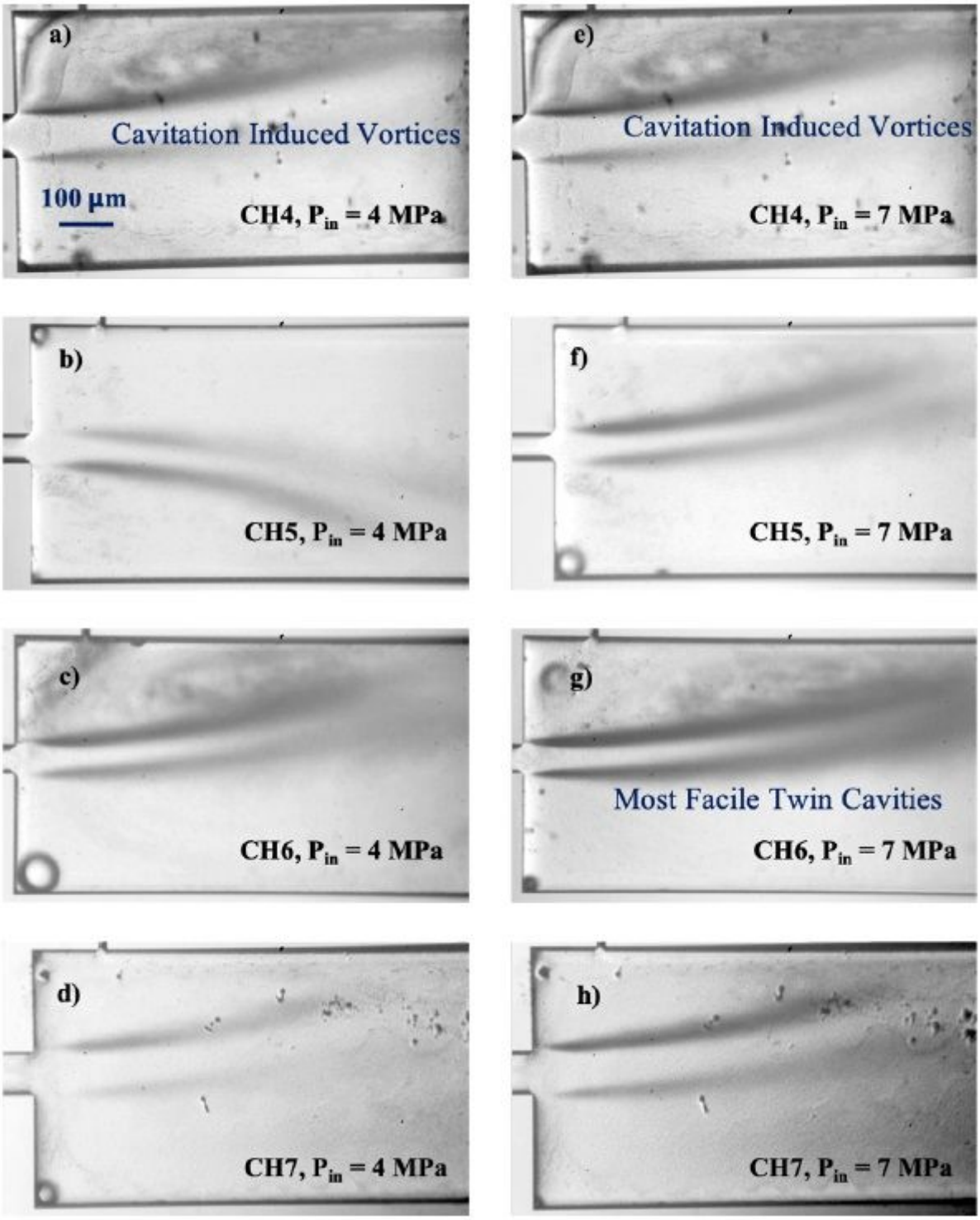

Figure 7

The twin cavities in the extension part of the four side wall roughened microfluidic devices at upstream pressures (Pin) of 4 and 7 MPa

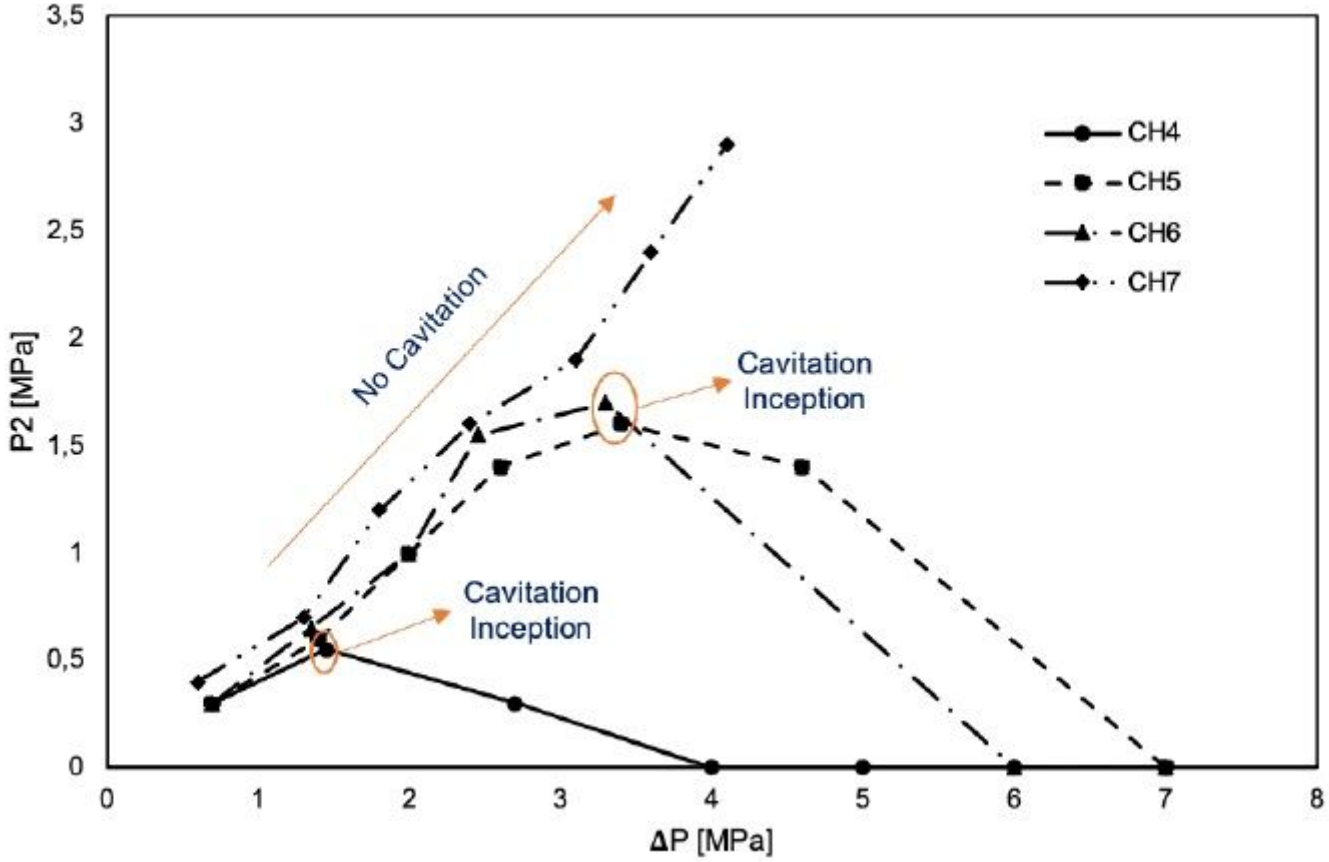

Figure 8

The variation of the P2, the pressure at the location of the vena contracta with respect to the pressure drop for four side wall roughened microfluidic devices

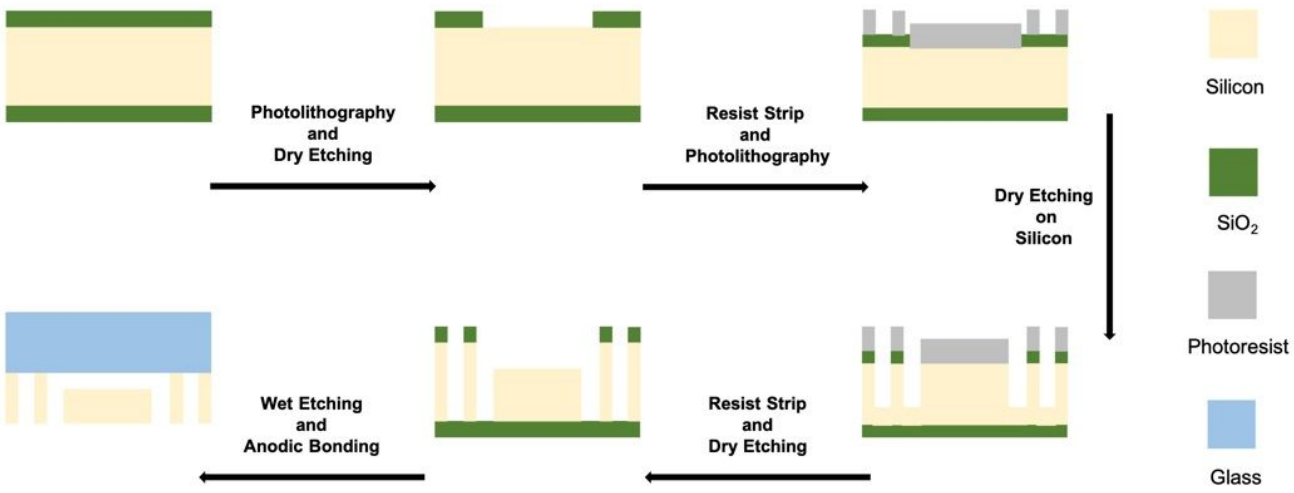

Figure 9

The process flow presenting the manufacturing process of the microfluidic devices

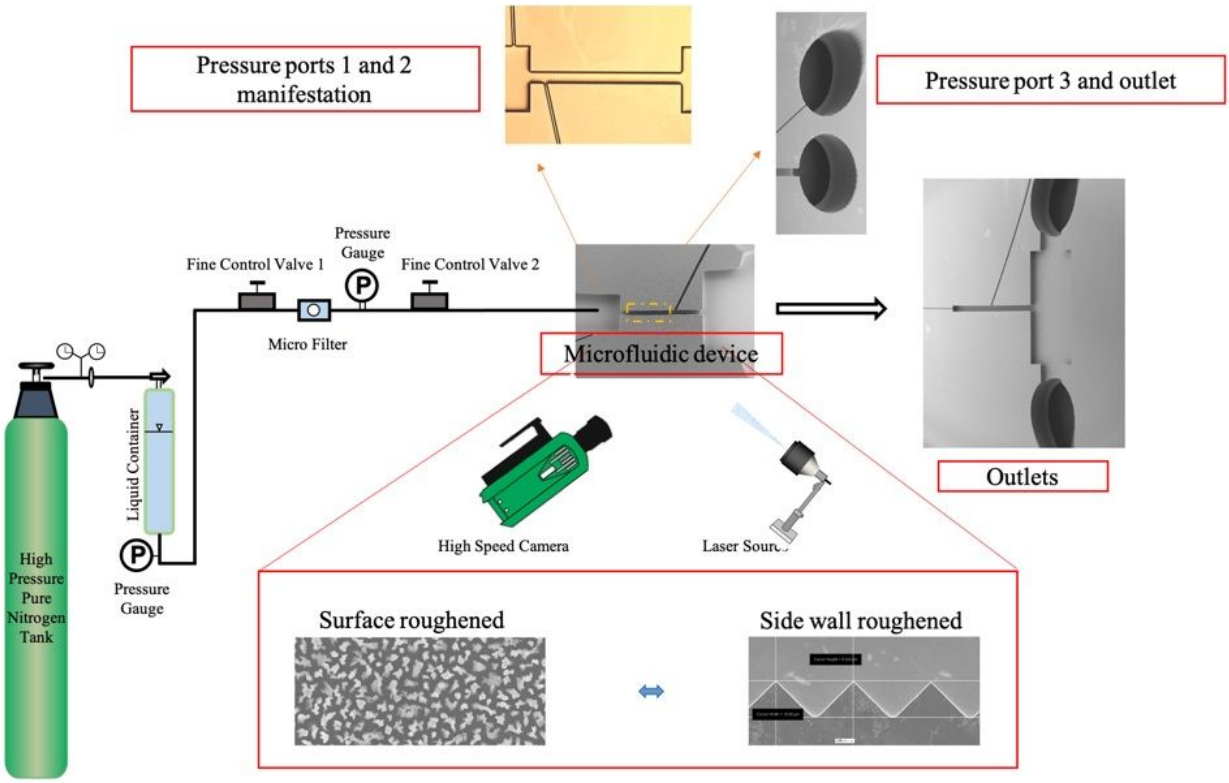

Figure 10

The experimental setup schematic illustrating the component required for the creation of the hydrodynamic cavitation phenomenon in a microfluidic device; The measured pressure in port 1 is Pin which is upstream pressure (also used as the reference pressure in the cavitation number formula), the P2 is measured at port 2, and the pressure measured at port 3 is approximately atmospheric pressure in all the cases.